Robust Control of the Safety Factor Profile and Stored Energy Evolutions in High Performance Burning Plasma Scenarios in the ITER Tokamak

Justin E. Barton, Karim Besseghir, Jo Lister and Eugenio Schuster

***Abstract*— The next step towards the development of a nuclear fusion tokamak power plant is the ITER project. Integrated closed-loop control of the plasma stored energy and safety factor profile (q-profile) is key to maintaining the plasma in a stable state and maximizing its performance. The q-profile evolution in tokamaks is related to the poloidal magnetic flux profile evolution, which is described by a physics model called the magnetic diffusion equation. A first-principles-driven (FPD), nonlinear, control-oriented model of the poloidal magnetic flux profile evolution is obtained by first combining the magnetic diffusion equation with simplified physics-based models of the noninductive current-drives. Secondly, the electron density, electron temperature, and plasma resistivity profiles are modeled as uncertain parameters by defining ranges in which they are expected to be in typical ITER high performance scenarios. This FPD model is then employed to synthesize an H_∞ feedback algorithm that utilizes ITER's auxiliary heating/current-drive sources and the total plasma current as actuators to control the q-profile and stored energy in high performance burning plasma scenarios while ensuring the closed-loop system is robust to the uncertainties in the plasma parameters. Finally, the effectiveness of the controller is demonstrated through simulation.**

I. Introduction

The tokamak is a magnetic confinement device used to heat and confine a reactant gas (a deuterium-tritium mixture), which is in a plasma state, to produce energy via nuclear fusion [1]. The next phase of tokamak development is the ITER project [2]. In order for ITER to meet its performance objectives, extensive research has been conducted to find high performance operating scenarios characterized by a high fusion gain, plasma stability, and a noninductively driven plasma current [3]. The safety factor profile, or q-profile, (defined as the ratio between the number of times a magnetic field line goes toroidally (the long way) around the tokamak to the number of times it goes around poloidally (the short way)) affects both the stability and performance of the plasma. Therefore, closed-loop control of the q-profile to drive it to a desirable target evolution is key to sustaining high performance scenarios. To optimize the fusion power generated by the reactor, the density and temperature profiles must also simultaneously be controlled. The volume-averaged plasma stored energy is related to these kinetic profiles and can be controlled to regulate the fusion power.

This work was supported by the National Science Foundation CAREER Award (ECCS-0645086), the U.S. Department of Energy (DE-FG02-09ER55064) and the Fonds National Suisse de la Recherche Scientifique. J. Barton (justin.barton@lehigh.edu) and E. Schuster are with the Department of Mechanical Engineering and Mechanics, Lehigh University, Bethlehem, PA 18015, USA. K. Besseghir and J. Lister are with the École Polytechnique Fédérale de Lausanne (EPFL), Centre de Recherches en Physique des Plasmas (CRPP), Association EURATOM-Suisse, 1015 Lausanne, Switzerland.

Recent experiments at DIII-D [4]–[6] represent the first successful demonstration of first-principles-driven (FPD), model-based, closed-loop control of the entire q-profile in a tokamak, where the control strategy employed was a feedforward + feedback scheme. Other advances towards designing FPD controllers to control the plasma magnetic profile are discussed in [7]–[9]. In the DIII-D experiments, the closed-loop control was chosen to be performed in low confinement (L-mode) [1] scenarios due to the reduced complexity of the plasma dynamics in this regime. In this work, we extend the control strategy employed in [4]–[6] to control the q-profile and stored energy in high performance, high confinement (H-mode) [1] burning plasma, i.e., one with a significant number of fusion reactions occurring, regimes in ITER. A profile control algorithm based on real-time estimation of linearized plasma profile response models for ITER is discussed in [10].

High confinement scenarios in tokamaks are characterized by transport barriers [1] just inside the plasma boundary that increase the coupling between the magnetic and kinetic states through the increase of the bootstrap current (a self-generated current) [11]. In the companion paper [12], a control-oriented partial differential equation (PDE) model of the poloidal magnetic flux profile evolution, which is related to the q-profile, valid for H-mode scenarios is developed. In this work, the model is utilized to design an integrated robust feedback control algorithm that employs ITER's auxiliary heating/current-drive sources (three electron cyclotron (gyrotron) launchers, one ion cyclotron launcher, one total neutral beam power launcher) and the total plasma current as actuators to track a desired target q-profile and stored energy evolution. The controller is designed to be robust to uncertainties in the electron density, electron temperature, and plasma resistivity profiles, which are modeled as uncertain parameters by defining ranges in which they are expected to be in typical ITER high performance scenarios. In the scenarios considered in this work, the ion cyclotron launcher is configured to provide only heating power to the plasma. Therefore, we design the algorithm with a two loop structure. The first loop utilizes the gyrotron and neutral beam launchers and the total plasma current to control the q-profile, and the second loop utilizes the ion cyclotron launcher to control the stored energy. Finally, the effectiveness of the controller is demonstrated through simulation with the FPD model developed in [12].

II. Plasma State Evolution Models

Any arbitrary quantity that is constant on each magnetic flux surface within the tokamak plasma can be used to

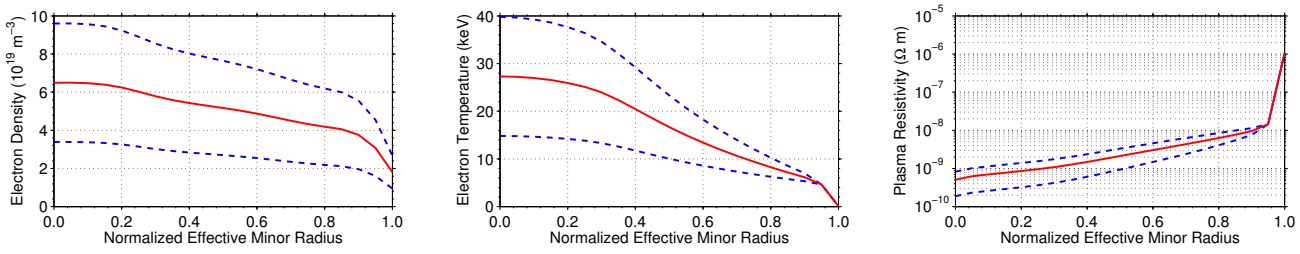

(a) (b) (c)

Fig. 1. Plasma parameter uncertainty ranges: (a) electron density, (b) electron temperature, and (c) plasma resistivity. Note: nominal values (solid) and minimum/maximum values (dash).

index the magnetic flux surfaces. In this work, we choose the mean effective minor radius, ρ, of the magnetic flux surface, i.e., $\pi B_{\phi,0}\rho^2 = \Phi$, as the indexing variable, where Φ is the toroidal magnetic flux and $B_{\phi,0}$ is the vacuum toroidal magnetic field at the geometric major radius R_0 of the tokamak. The normalized effective minor radius is defined as $\hat{\rho} = \rho/\rho_b$, where ρ_b is the mean effective minor radius of the last closed magnetic flux surface. Simplified physics-based models of the noninductive current-drives are discussed in [12]. The auxiliary noninductive current-drives are proportional to the current-drive efficiency T_e/n_e, where T_e and n_e are the electron temperature and density profiles, respectively, and the bootstrap current-drive is proportional to the inverse of the poloidal magnetic flux gradient profile multiplied by the kinetic plasma profile gradients.

We begin by defining ranges in which the electron density and temperature profiles are expected to be in typical ITER high performance scenarios, which are shown in Figs. 1(a)-(b). We model these kinetic parameters as a nominal profile plus a bounded uncertain profile, i.e.,

$$n_e(\hat{\rho},t) = n_e^{nom}(\hat{\rho}) + n_e^{unc}(\hat{\rho})\delta_{n_e}, \tag{1}$$

$$T_e(\hat{\rho},t) = T_e^{nom}(\hat{\rho}) + T_e^{unc}(\hat{\rho})\delta_{T_e}, \tag{2}$$

where $n_e^{nom}(\hat{\rho}) = \left[n_e^{max}(\hat{\rho}) + n_e^{min}(\hat{\rho})\right]/2$, $T_e^{nom}(\hat{\rho}) = \left[T_e^{max}(\hat{\rho}) + T_e^{min}(\hat{\rho})\right]/2$, $n_e^{unc}(\hat{\rho}) = \left[n_e^{max}(\hat{\rho}) - n_e^{min}(\hat{\rho})\right]/2$, and $T_e^{unc}(\hat{\rho}) = \left[T_e^{max}(\hat{\rho}) - T_e^{min}(\hat{\rho})\right]/2$, with $|\delta_{T_e}| \le 1$ and $|\delta_{n_e}| \le 1$. The plasma resistivity decreases as the electron temperature increases, therefore, the minimum resistivity is defined by the maximum electron temperature, and the maximum resistivity is defined by the minimum electron temperature, which are shown in Fig. 1(c). The inverse of the electron density is related to the electron density in the same manner. These plasma parameters are modeled as

$$\eta(\hat{\rho},t) = \eta^{nom}(\hat{\rho}) + \eta^{unc}(\hat{\rho})\delta_{T_e}, \tag{3}$$

$$1/n_e(\hat{\rho},t) = n_e^{nom'}(\hat{\rho}) + n_e^{unc'}(\hat{\rho})\delta_{n_e}, \tag{4}$$

where $\eta^{nom}(\hat{\rho}) = \left[\eta^{max}(\hat{\rho}) + \eta^{min}(\hat{\rho})\right]/2$, $n_e^{nom'}(\hat{\rho}) = \left[n_e^{max}(\hat{\rho}) + n_e^{min}(\hat{\rho})\right] / \left[2n_e^{max}(\hat{\rho})n_e^{min}(\hat{\rho})\right]$, $\eta^{unc}(\hat{\rho}) = \left[\eta^{min}(\hat{\rho}) - \eta^{max}(\hat{\rho})\right]/2$, and $n_e^{unc'}(\hat{\rho}) = \left[n_e^{min}(\hat{\rho}) - n_e^{max}(\hat{\rho})\right] / \left[2n_e^{max}(\hat{\rho})n_e^{min}(\hat{\rho})\right]$.

The q-profile is related to the poloidal stream function ψ, which is closely related to the poloidal magnetic flux Ψ ($\Psi = 2\pi\psi$), and is defined as $q(\hat{\rho},t) = -d\Phi/d\Psi = -\left[B_{\phi,0}\rho_b^2\hat{\rho}\right] / \left[\partial\psi/\partial\hat{\rho}\right]$. Therefore, if we are able to control the poloidal flux gradient profile, which we define as

$$\theta(\hat{\rho},t) \equiv \partial\psi/\partial\hat{\rho}(\hat{\rho},t), \tag{5}$$

we will be able to control the q-profile, assuming the system is controllable. By combining the physics model that describes the poloidal magnetic flux profile evolution in the tokamak (the magnetic diffusion equation [13], [14]) with the noninductive current-drive models [12] and the models (1)-(4), the PDE governing the evolution of θ is given by

$$\begin{aligned}
\frac{\partial\theta}{\partial t} = {} & \left[q_1(\hat{\rho}) + q_4(\hat{\rho})\delta_{T_e}\right]\frac{\partial^2\theta}{\partial\hat{\rho}^2} + \left[q_2(\hat{\rho}) + q_5(\hat{\rho})\delta_{T_e}\right]\frac{\partial\theta}{\partial\hat{\rho}} \\
& + \left[q_3(\hat{\rho}) + q_6(\hat{\rho})\delta_{T_e}\right]\theta \\
& + \left[g_1'(\hat{\rho}) + h_1'(\hat{\rho})\delta_{n_e} + k_1'(\hat{\rho})\delta_{T_e} + l_1'(\hat{\rho})\delta_{T_e}\delta_{n_e}\right. \\
& \left. + m_1'(\hat{\rho})\delta_{T_e}^2 + p_1'(\hat{\rho})\delta_{T_e}^2\delta_{n_e}\right]P_{ec_1}(t) \\
& + \left[g_2'(\hat{\rho}) + h_2'(\hat{\rho})\delta_{n_e} + k_2'(\hat{\rho})\delta_{T_e} + l_2'(\hat{\rho})\delta_{T_e}\delta_{n_e}\right. \\
& \left. + m_2'(\hat{\rho})\delta_{T_e}^2 + p_2'(\hat{\rho})\delta_{T_e}^2\delta_{n_e}\right]P_{ec_2}(t) \\
& + \left[g_3'(\hat{\rho}) + h_3'(\hat{\rho})\delta_{n_e} + k_3'(\hat{\rho})\delta_{T_e} + l_3'(\hat{\rho})\delta_{T_e}\delta_{n_e}\right. \\
& \left. + m_3'(\hat{\rho})\delta_{T_e}^2 + p_3'(\hat{\rho})\delta_{T_e}^2\delta_{n_e}\right]P_{ec_3}(t) \\
& + \left[g_4'(\hat{\rho}) + h_4'(\hat{\rho})\delta_{n_e} + k_4'(\hat{\rho})\delta_{T_e} + l_4'(\hat{\rho})\delta_{T_e}\delta_{n_e}\right. \\
& \left. + m_4'(\hat{\rho})\delta_{T_e}^2 + p_4'(\hat{\rho})\delta_{T_e}^2\delta_{n_e}\right]P_{nbi}(t) \\
& - \left[g_5(\hat{\rho}) + h_5(\hat{\rho})\delta_{n_e} + k_5(\hat{\rho})\delta_{T_e} + l_5(\hat{\rho})\delta_{T_e}\delta_{n_e}\right. \\
& \left. + m_5(\hat{\rho})\delta_{T_e}^2 + p_5(\hat{\rho})\delta_{T_e}^2\delta_{n_e}\right]\left(\frac{1}{\theta}\right)^2\frac{\partial\theta}{\partial\hat{\rho}} \\
& + \left[g_5'(\hat{\rho}) + h_5'(\hat{\rho})\delta_{n_e} + k_5'(\hat{\rho})\delta_{T_e} + l_5'(\hat{\rho})\delta_{T_e}\delta_{n_e}\right. \\
& \left. + m_5'(\hat{\rho})\delta_{T_e}^2 + p_5'(\hat{\rho})\delta_{T_e}^2\delta_{n_e}\right]\left(\frac{1}{\theta}\right),
\end{aligned} \tag{6}$$

with boundary conditions

$$\theta(0,t) = 0 \qquad \theta(1,t) = -k_7 I(t), \tag{7}$$

where t is the time, $(\cdot)' = d/d\hat{\rho}$, the parameters $q_i(\hat{\rho})$ for $i = 1,\ldots,6$ and $g_j(\hat{\rho})$, $h_j(\hat{\rho})$, $k_j(\hat{\rho})$, $l_j(\hat{\rho})$, $m_j(\hat{\rho})$, and $p_j(\hat{\rho})$ for $j = 1,\ldots,5$ are functions of space, k_7 is a constant, $P_{ec_i}(t)$ for $i = 1,2,3$ is each gyrotron launcher power, $P_{nbi}(t)$ is the total neutral beam power, and $I(t)$ is the total plasma current.

The volume-averaged energy balance in the plasma is given by

$$\frac{d\bar{W}}{dt} = -\frac{\bar{W}}{\tau_{\bar{W}}} + P_{ec_1} + P_{ec_2} + P_{ec_3} + P_{ic} + P_{nbi} - P_{rad} + P_{\alpha}, \tag{8}$$

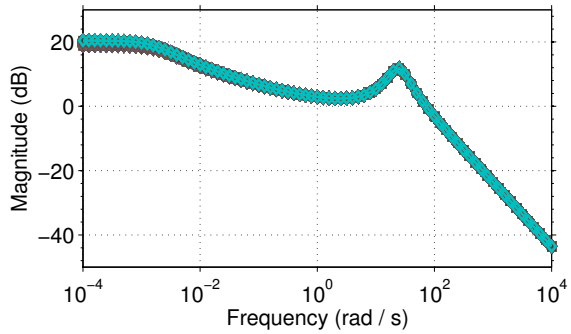

Fig. 2. Magnitude of maximum singular value versus frequency of the linear model (11) along the nonlinear feedforward state and control input trajectories $x_{ff}(t)$ and $u_{ff}(t)$ for $\delta = 0$ and $d = 0$.

where $\bar{W}$ is the volume-averaged stored energy, $\tau_{\bar{W}}$ is the global energy confinement time, P_{ic} is the ion cyclotron launcher power, P_{rad} is the radiated power, and P_{α} is the heating power generated by fusion reactions. The energy confinement time scaling used in this work is the IPB98(y,2) scaling law [15].

III. Model Reduction via Spatial Discretization

To construct a reduced-order model suitable for feedback control design, the governing PDE (6) is discretized in space using a finite difference method, where the spatial domain of interest, $\hat{\rho} \in [0,1]$, is represented as l nodes. After applying the spatial derivative approximations to (6) and taking into account the boundary conditions (7), we obtain a nonlinear, finite dimensional, ordinary differential equation model defined by

$$\dot{x} = w(x,u,\delta), \tag{9}$$

where $x = [\theta_2, \theta_3, \ldots, \theta_{l-1}]^T \in \mathbb{R}^{n\times 1}$ is the state vector, θ_i is the value of θ at the discrete nodes, $u = [P_{ec_1}, P_{ec_2}, P_{ec_3}, P_{nbi}, I]^T \in \mathbb{R}^{5\times 1}$ is the control input vector, $\delta = \left[\delta_{T_e}, \delta_{n_e}, \delta_{T_e}\delta_{n_e}, \delta_{T_e}^2, \delta_{T_e}^2\delta_{n_e}\right] \in \mathbb{R}^{5\times 1}$ is the uncertain parameter vector, $w \in \mathbb{R}^{n\times 1}$ is a nonlinear function of the model parameters, the system states, the control inputs, and uncertain parameters, $n = l-2$, and

$$\theta_1(t) = 0 \qquad \theta_l(t) = -k_7 I(t).$$

Let $x_{ff}(t)$, $u_{ff}(t)$, and $\delta_{ff}(t)$ be a set of feedforward system trajectories, which satisfy

$$\dot{x}_{ff} = w(x_{ff}, u_{ff}, \delta_{ff}). \tag{10}$$

We can obtain a model suitable for tracking control design by defining the perturbation variables $\tilde{x}(t) = x(t) - x_{ff}(t)$ and $u_{fb}(t) = u(t) - u_{ff}(t)$, where $\tilde{x}(t)$ is the deviation away from the feedforward state trajectories and $u_{fb}(t)$ is the output of the to-be-designed feedback controller. Linearizing (9) with respect to the state and control input and using (10), we obtain a linear time-variant (LTV) system given by

$$\dot{\tilde{x}} = \left.\frac{\partial w}{\partial x}\right|_{(x_{ff},u_{ff})} \tilde{x} + \left.\frac{\partial w}{\partial u}\right|_{(x_{ff},u_{ff})} u_{fb} + d(t), \tag{11}$$

where $\partial w/\partial x \in \mathbb{R}^{n\times n}$ and $\partial w/\partial u \in \mathbb{R}^{n\times 5}$ are the system Jacobians, which depend on the uncertain parameters as

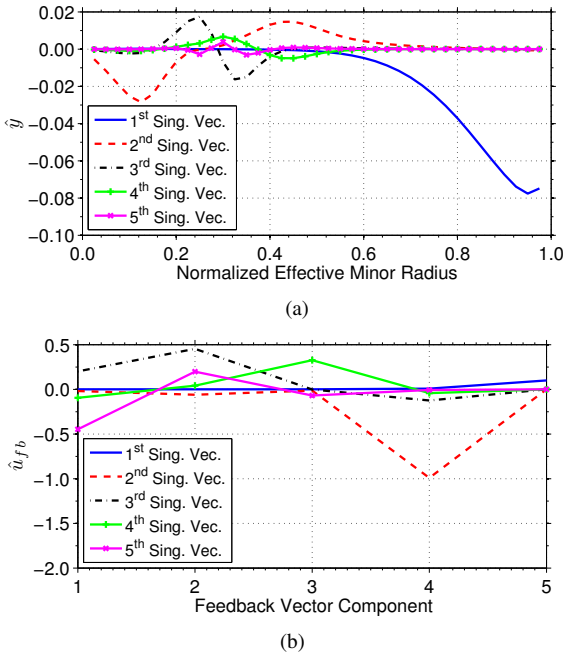

Fig. 3. Relevant control channels: (a) output and (b) input.

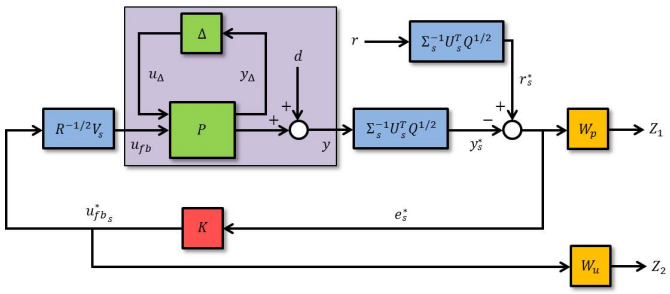

Fig. 4. Schematic of q-profile feedback control problem formulation.

well as the feedforward state and input trajectories, and $d(t) = w(x_{ff}, u_{ff}, \delta) - w(x_{ff}, u_{ff}, \delta_{ff})$. Figure 2 shows the maximum singular value versus frequency of the linear model (11) along the nonlinear feedforward state and control input trajectories for $\delta = 0$ and $d = 0$. As shown in the figure, the dynamic response of the system is weakly dependent on the feedforward state and input trajectories. Therefore, we evaluate the Jacobians at a specific feedforward state and input to obtain a linear time-invariant (LTI) model of the deviation dynamics given by

$$\dot{\tilde{x}} = A\tilde{x} + Bu_{fb} + d \qquad y = C\tilde{x} + Du_{fb}, \tag{12}$$

with

$$A = A_0 + \sum_{m=1}^{5} \delta_m A_m \qquad B = B_0 + \sum_{m=1}^{5} \delta_m B_m,$$
$$C = C_0 + \sum_{m=1}^{5} \delta_m C_m \qquad D = D_0 + \sum_{m=1}^{5} \delta_m D_m, \tag{13}$$

where A_i and B_i for $i = 0, \ldots, 5$ are the Jacobians evaluated at a specific feedforward state and input, C_0 is an $n \times n$ identity matrix, $D_0 = 0$, and $C_j = 0$ and $D_j = 0$ for $j = 1, \ldots, 5$. In this work, we assume the plasma state is measurable.

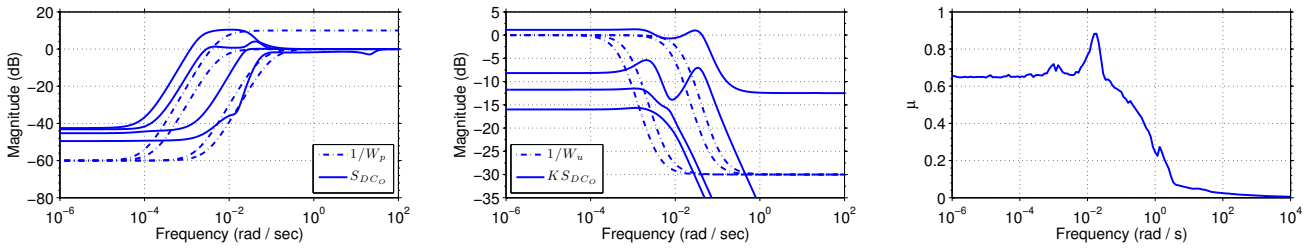

(a) (b) (c)

Fig. 5. Singular value diagrams: (a) $1/W_p$ (dash-dotted) and S_{DC_o} (solid) and (b) $1/W_u$ (dash-dotted) and KS_{DC_o} (solid), and (c) μ versus frequency.

A. Model in Robust Control Framework

The transfer function of a linear system with state-space matrices A, B, C, and D can be written as an upper linear fractional transformation (LFT) as $G(s) = F_u(M_a, [1/s]I_n) = D + C(sI_n - A)^{-1}B$, where F_u denotes the upper LFT, the matrix M_a is defined as

$$M_a = \begin{bmatrix} A & B \\ C & D \end{bmatrix},$$

I_n is an $n \times n$ identity matrix, and s denotes the Laplace variable. The system can be expressed in the conventional $P-\Delta$ control framework by employing the method outlined in [16], which exploits the structure of the state matrices in (13). See [4] for an example of this technique. If the plant $P \in \mathbb{R}^{(q_T+n)\times(q_T+5)}$, where q_T is the rank of the structured uncertainty matrix $\Delta = \text{diag}\{\delta\}$, is partitioned as

$$P = \begin{bmatrix} P_{11} & P_{12} \\ P_{21} & P_{22} \end{bmatrix},$$

the input-output equations of the system are

$$y_\Delta = P_{11}u_\Delta + P_{12}u_{fb} \qquad y = P_{21}u_\Delta + P_{22}u_{fb} + d, \quad (14)$$

where $P_{11} \in \mathbb{R}^{q_T \times q_T}$, $P_{12} \in \mathbb{R}^{q_T \times 5}$, $P_{21} \in \mathbb{R}^{n \times q_T}$, $P_{22} \in \mathbb{R}^{n \times 5}$, $y_\Delta \in \mathbb{R}^{q_T \times 1}$, $u_\Delta \in \mathbb{R}^{q_T \times 1}$, $y \in \mathbb{R}^{n \times 1}$, $d \in \mathbb{R}^{n \times 1}$, and $u_{fb} \in \mathbb{R}^{5 \times 1}$.

IV. Identification of Relevant Control Channels

It is desired that the output y be able to track a reference value r, therefore, we define the tracking error as $e = r - y$. As there are only five inputs, we can only independently control five linear combinations of the output of the system, and we employ a singular value decomposition of the nominal state-space system A_0, B_0, C_0, D_0 at a particular frequency to identify the most relevant control channels. The relationship between the outputs y and inputs u_{fb} of the nominal system is expressed as $y = G_0(s)u_{fb}$, where $G_0(s) = C_0(sI_n - A_0)^{-1}B_0 + D_0$ is the nominal transfer function.

The real approximation of the nominal input-output relation at a particular frequency $j\omega_{dc}$ is expressed as

$$\hat{y} = \hat{G}_0 \hat{u}_{fb}, \quad (15)$$

where $\hat{y}$ denotes the decoupled/relevant output, $\hat{u}_{fb}$ denotes the decoupled/relevant input, and $\hat{G}_0$ denotes the real approximation of the complex matrix $G_0(j\omega_{dc})$ [17]. We select the frequency to identify the relevant channels at as $\omega_{dc} = 10^{-1}$ rad/sec., which allows us to utilize the plasma current to control the q-profile near the plasma boundary and the gyrotron launchers and the neutral beam injectors to control the q-profile evolution near the center of the plasma. In order to weight the tracking performance and control effort, we introduce the positive definite weighting matrices $Q \in \mathbb{R}^{n \times n}$ and $R \in \mathbb{R}^{5 \times 5}$, and we define the "weighted" transfer function $\tilde{G}_0$ and its economy size singular value decomposition as $\tilde{G}_0 = Q^{1/2}\hat{G}_0 R^{-1/2} = U\Sigma V^T$, where $\Sigma = \text{diag}(\sigma_1, \sigma_2, \sigma_3, \sigma_4, \sigma_5) \in \mathbb{R}^{5 \times 5}$ is a diagonal matrix of singular values and $U \in \mathbb{R}^{n \times 5}$ and $V \in \mathbb{R}^{5 \times 5}$ are matrices that possess the following properties $V^TV = VV^T = I, U^TU = I$, where I is a 5×5 identity matrix, and $(\cdot)^T$ denotes the matrix transpose. The input-output relation (15) is now expressed as

$$\hat{y} = Q^{-1/2}\tilde{G}_0 R^{1/2}\hat{u}_{fb} = Q^{-1/2}U\Sigma V^T R^{1/2}\hat{u}_{fb}.$$

The singular vectors of the basis for the subspace of obtainable output values ($\hat{y} = Q^{-1/2}U\Sigma\hat{y}^*$), and hence the trackable components of the reference vector $\hat{r}$, as well as the corresponding input singular vectors ($\hat{u}_{fb} = R^{-1/2}V\hat{u}^*_{fb}$) are shown in Fig. 3. As the magnitude of the singular value σ_i decreases, a larger amount of control effort is needed to produce a significant contribution to the profile. To avoid spending a lot of control effort for only a small improvement in the value of the tracking error $\left(\hat{e} = \hat{r} - \hat{y} = Q^{-1/2}U\Sigma(\hat{r}^* - \hat{y}^*)\right)$, we can partition the singular values into k significant singular values Σ_s and $5-k$ negligible singular values Σ_{ns} and define the significant components of the reference, output, and input vectors as $\hat{r}^*_s = \Sigma_s^{-1}U_s^T Q^{1/2}\hat{r} \in \mathbb{R}^{k \times 1}$, $\hat{y}^*_s = \Sigma_s^{-1}U_s^T Q^{1/2}\hat{y} \in \mathbb{R}^{k \times 1}$, and $\hat{u}^*_{fb_s} = V_s^T R^{1/2}\hat{u}_{fb} \in \mathbb{R}^{k \times 1}$, where $U_s \in \mathbb{R}^{n \times k}$ and $V_s \in \mathbb{R}^{5 \times k}$ are the components of U and V associated with the significant singular values. More details regarding this technique can be found in [4], [18].

V. Integrated Feedback Controller Synthesis

We now synthesize an integrated control algorithm to simultaneously control the q-profile and stored energy evolutions. We use the gyrotron launchers, neutral beam injectors, and total plasma current to control the q-profile, and we use the ion cyclotron launcher to control the stored energy.

A. Safety Factor Profile Controller Design

The control goal is to design a feedback controller that can minimize the tracking error, $e = r - y$, while using as little feedback control effort as possible, achieve a set of specified performance objectives, and robustly stabilize the

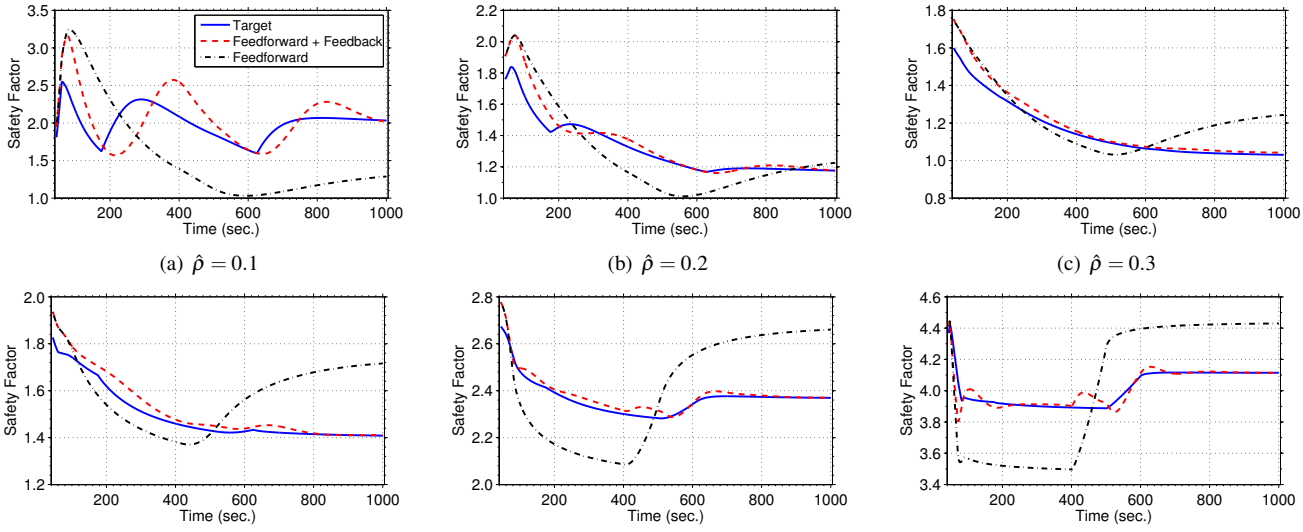

(a) $\hat{\rho} = 0.1$ (b) $\hat{\rho} = 0.2$ (c) $\hat{\rho} = 0.3$

(d) $\hat{\rho} = 0.5$ (e) $\hat{\rho} = 0.7$ (f) $\hat{\rho} = 0.9$

Fig. 6. Time trace of safety factor q at various spatial locations. Note: target (solid), feedforward + feedback (dash), and feedforward (dash-dotted).

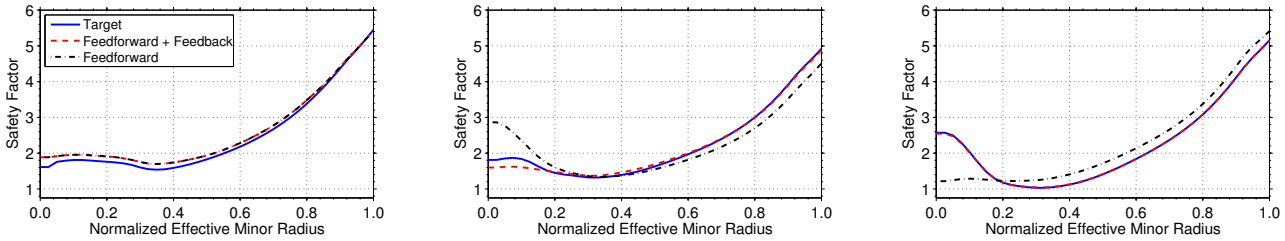

(a) $t = 45$ sec. (b) $t = 195$ sec. (c) $t = 995$ sec.

Fig. 7. Safety factor profile $q(\hat{\rho})$ at various times during the simulations.

system by controlling the relevant channels of the system (14). This control problem is shown in Fig. 4, where K is the feedback controller, $Z_1 = W_p e_s^*$, $Z_2 = W_u u_{fb_s}^*$, and W_p and W_u are frequency dependent weight functions used to optimize the closed-loop performance. The nominal performance condition of the closed-loop system is expressed as

$$\begin{bmatrix} Z_1 \\ Z_2 \end{bmatrix} = \begin{bmatrix} W_p S_{DC_O} & -W_p S_{DC_O} \\ W_u K S_{DC_O} & -W_u K S_{DC_O} \end{bmatrix} \begin{bmatrix} \bar{r}_s^* \\ \bar{d}_s^* \end{bmatrix} = T_{zw} \begin{bmatrix} \bar{r}_s^* \\ \bar{d}_s^* \end{bmatrix},$$

where $S_{DC_O} = (I + \Sigma_s^{-1} U_s^T Q^{1/2} P_{22} R^{-1/2} V_s K)^{-1}$. Therefore, the control problem is formulated as

$$\min_K \left|\left| T_{zw} \right|\right|_\infty, \quad \forall \omega. \tag{16}$$

The feedback controller K found by solving (16) is written in state-space form as

$$\dot{x}_{fb} = A_{fb} x_{fb} + B_{fb} e_s^* \qquad u_{fb_s}^* = C_{fb} x_{fb} + D_{fb} e_s^*, \tag{17}$$

where the vector $x_{fb} \in \mathbb{R}^{p \times 1}$ is the internal controller states, $A_{fb} \in \mathbb{R}^{p \times p}$, $B_{fb} \in \mathbb{R}^{p \times k}$, $C_{fb} \in \mathbb{R}^{k \times p}$, and $D_{fb} \in \mathbb{R}^{k \times k}$ are the controller system matrices, and p is the number of controller states. As the uncertainty has a block-diagonal structure, i.e., $\Delta = \text{diag}\{\delta\}$, we can compute the structured singular value $\mu\big(N_{11}(j\omega)\big)$ to determine the robust stability of the closed-loop system, where N_{11} is the transfer function between y_Δ and u_Δ. The closed-loop system is robustly stable for all allowable perturbations if and only if $\mu\big(N_{11}(j\omega)\big) < 1$, $\forall \omega$ [17]. To analyze the performance and robust stability of the closed-loop system, the singular value diagrams of the inverse of the performance weight functions and the achieved transfer functions S_{DC_O} and KS_{DC_O} are shown in Figs. 5(a)-(b) and a plot of μ versus frequency is shown in Fig. 5(c).

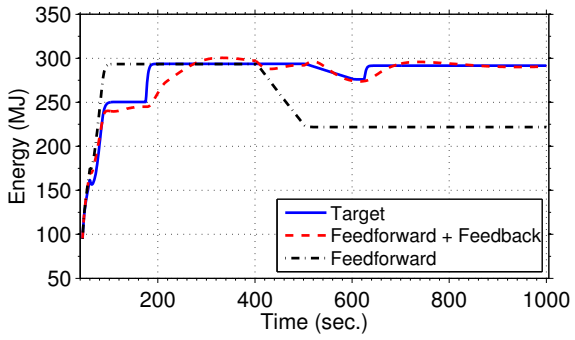

Fig. 8. Plasma stored energy versus time.

B. Plasma Stored Energy Controller Design

The ion cyclotron launcher is used in a feedforward + feedback scheme, i.e., $P_{ic} = P_{ic_{ff}} + P_{ic_{fb}}$, where $P_{ic_{ff}}$ and $P_{ic_{fb}}$ are the feedforward and feedback components, to control the stored energy. The feedback controller is expressed as

$$P_{ic_{fb}} = k_{P_{ic}} e_{\bar{W}} + k_{I_{ic}} \int_0^t e_{\bar{W}} dt, \tag{18}$$

where $k_{P_{ic}}$ and $k_{I_{ic}}$ are the controller gains, $e_{\bar{W}} = \bar{W}_{tar} - \bar{W}$ is the error in the stored energy, and $\bar{W}_{tar}$ is the reference.

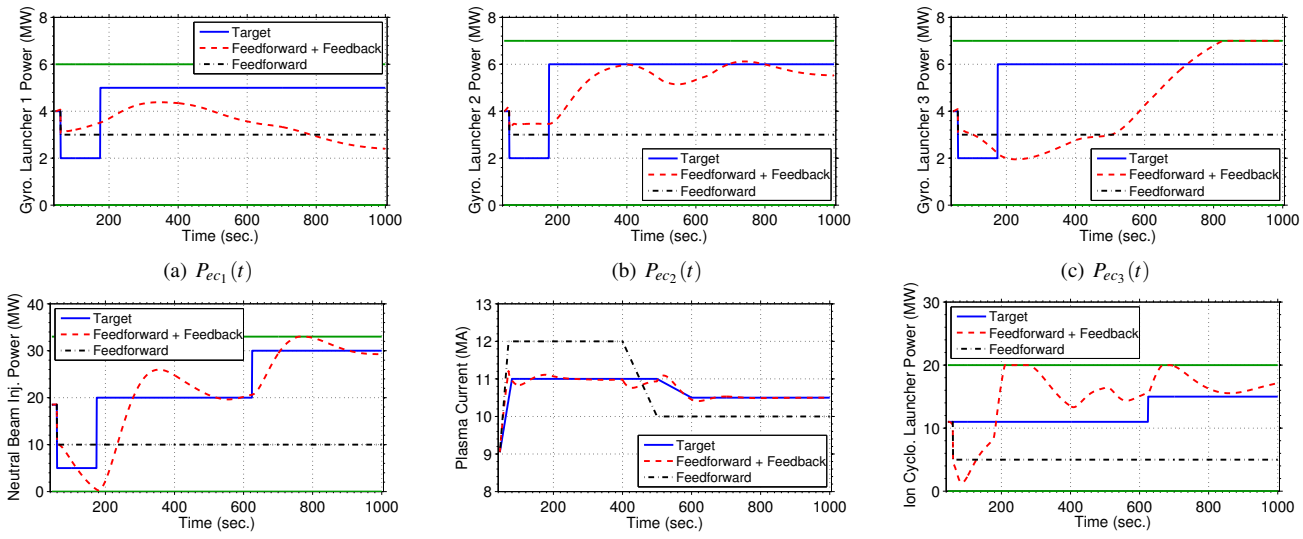

(a) $P_{ec_1}(t)$ (b) $P_{ec_2}(t)$ (c) $P_{ec_3}(t)$

(d) $P_{nbi}(t)$ (e) $I(t)$ (f) $P_{ic}(t)$

Fig. 9. Control trajectory comparison: (a)-(c) individual gyrotron launcher powers, (d) neutral beam injection power, (e) total plasma current, and (f) ion cyclotron launcher power. The actuator magnitude limits are shown in solid-green.

VI. Simulation Testing of Control Algorithm

The integrated feedback controller (17)-(18) is now tested through simulation with the FPD, physics-based model of the poloidal magnetic flux profile evolution developed in [12] and the volume-averaged plasma energy balance (8) tailored to H-mode burning plasma scenarios in ITER. First, a target q-profile and stored energy evolution is obtained by executing a feedforward-only simulation with a nominal set of input trajectories and initial conditions $q_{nom}(\hat{\rho},t_0)$ and $\bar{W}_{nom}(t_0)$, where $t_0 = 45$ sec. is the time just after the plasma transitions from L-mode to H-mode in this particular simulated scenario. Second, a different q-profile and stored energy evolution is obtained by executing a feedforward-only simulation with a perturbed set of input trajectories and initial conditions. Finally, the ability of the algorithm to track the target evolutions is determined by executing a feedforward + feedback simulation with the perturbed input trajectories and initial conditions. To ensure the closed-loop system remains well behaved in the presence of actuator magnitude saturation, the controller is augmented with an anti-windup compensator. In each simulation, the volume-average electron density is linearly ramped up from an initial value of $\langle n_e \rangle_V(t_0) = 2.4 \times 10^{19}$ m^{-3} to a final value of $\langle n_e \rangle_V(86) = 6.6 \times 10^{19}$ m^{-3} and then held constant.

Time traces of q at various spatial locations are shown in Fig. 6 and a comparison of the target, feedforward + feedback controlled, and feedforward controlled q-profiles at various times is shown in Fig. 7. The stored energy and the control inputs as a function of time are shown in Figs. 8 and 9, respectively. As shown, the controller is able to drive the q-profile and stored energy to the target evolutions during both the transient and steady-state phases of the simulation.

VII. Conclusions and Future Work

An integrated feedback algorithm to control the q-profile and stored energy evolutions in high performance burning plasma scenarios in ITER was designed by employing a FPD model of the system. Our future work includes (i) testing the controller in the DINA-CH&CRONOS free-boundary tokamak simulation code [19] and (ii) tailoring the q-profile controller to the DIII-D tokamak geometry and experimentally testing the algorithm in DIII-D.

References

[1] WESSON, J., *Tokamaks*, Oxford, U.K.: Clarendon Press, 1997.

[2] ITER Organization, [Online]. Available: http://www.iter.org.

[3] TAYLOR, T. et al., Plasma Phys. and Control. Fusion **39** (1997) B47.

[4] BARTON, J. E., BOYER, M., SHI, W., SCHUSTER, E., et al., Nucl. Fusion **52** (2012) 123018.

[5] BOYER, M. D., BARTON, J. E., SCHUSTER, E., et al., Plasma Phys. Control. Fusion **55** (2013) 105007.

[6] BOYER, M. D., BARTON, J., SCHUSTER, E., et al., Backstepping Control of the Plasma Current Profile in the DIII-D Tokamak, in *American Control Conference Proceedings*, pp. 2996–3001, 2012.

[7] ARGOMEDO, F. B. et al., Model-based Control of the Magnetic Flux Profile in a Tokamak Plasma, in *49th IEEE Conference on Decision and Control*, pp. 6926–6931, 2010.

[8] GAYE, O. et al., Sliding Mode Stabilization of the Current Profile in Tokamak Plasmas, in *50th IEEE Conference on Decision and Control*, pp. 2638–2643, 2011.

[9] GAHLAWAT, A. et al., Bootstrap Current Optimization in Tokamaks using Sum-of-Squares Polynomials, in *51st IEEE Conference on Decision and Control*, pp. 4359–4365, 2012.

[10] KIM, S. H. and LISTER, J. B., Nuclear Fusion **52** (2012) 074002.

[11] PEETERS, A. G., Plasma Phys. and Control. Fusion **42** (2000) B231.

[12] BARTON, J. E., SHI, W., BESSEGHIR, K., LISTER, J., KRITZ, A., SCHUSTER, E., et al., Physics-based Control-oriented Modeling of the Safety Factor Profile Dynamics in High Performance Tokamak Plasmas, in *52nd IEEE Conference on Decision and Control*, (this conference), 2013.

[13] HINTON, F. and HAZELTINE, R., Rev. Mod. Phys. **48** (1976) 239.

[14] OU, Y., LUCE, T. C., SCHUSTER, E., et al., Fusion Engineering and Design **82** (2007) 1153.

[15] ITER Physics Basis, Nuclear Fusion **39** (1999) 2137.

[16] PACKARD, A., *Whats New with μ: Structured Uncertainty in Multivariable Control*, PhD thesis, Univ. of Calif., Berkeley, 1988.

[17] SKOGESTAD, S. and POSTLETHWAITE, I., *Multivariable Feedback Control Analysis and Design*, Wiley, New York, 2005.

[18] AMBROSINO, G. et al., IET Control Theory and Applications **1** (2007) 604.

[19] KIM, S. H. et al., Plasma Phys. and Control. Fusion **51** (2009) 105007.